Nanoscale

Accepted Manuscript

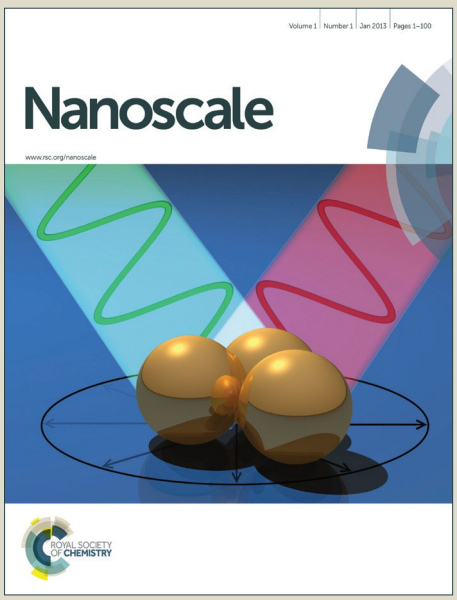

ROYAL SOCIETY OF CHEMISTRY

www.rsc.org/nanoscale

Journal Name

ARTICLE

Negative dissipation gradients in hysteretic materials

Miriam Jaafar[a†], Óscar Iglesias-Freire[a,b†], Pedro García-Mochales[c], Juan José Sáenz[d,e*] and Agustina Asenjo[a*]

Received 00th January 20xx,
Accepted 00th January 20xx

DOI: 10.1039/x0xx00000x

www.rsc.org/

Measuring energy dissipation on the nanoscale is of great interest not only for nanomechanics but also to understand important energy transformation and loss mechanisms that determines the efficiency of energy of data storage devices. Full understanding the magnetic dynamics and dissipation processes in nanomagnets is of major relevance for a number of basic and applied issues from magnetic recording to spin-based sensor devices and to biomedical magnetic-based hyperthermia treatments. Here we present experimental evidence for a counter-intuitive monotonical reduction of the energy dissipation as the interaction between two nanomagnets is enhanced. This behavior, which takes place when spins are parallel, can be understood in terms of hysteresis phenomena involved in the reorientation of this spins. Measured magnetic losses of about few femtowatts are in agreement with quasi-static micromagnetic numerical simulations.

Introduction

Fully understanding the magnetic dynamics and dissipation processes in nanometer-size ferromagnets is of major relevance for a number of basic and applied issues from magnetic recording to spin-based sensor devices and to biomedical magnetic-based hyperthermia treatments [1,2,3,4,5]. Scanning Probe Force Microscopy (SPM) provides a powerful tool to obtain dissipation maps at nanometer resolution by measuring the tiny amount of energy dissipated by a vibrating tip in the proximity of a sample surface [6,7,8]. The experimental determination of the spatial distribution of the energy dissipation allows short-range dissipation processes (adhesion, contact formation, capillary condensation, friction or wear) to be discriminated from long-range interactions as electrostatic and magnetostatic. In Magnetic Force Microscopy (MFM) configuration [9,10], -above certain tip-sample distance- the energy dissipated depends on the magnetic interactions between the tip and the sample i.e. on the relative orientation of tip and sample spins[9].

Dissipation in scanning force microscopy relies on extracting physical information by recording variations in the cantilever oscillation[7,11,12] , as some energy is transferred into dissipative processes. Multiple causes for this dissipation of energy have been experimentally determined, such as Joule heating [13], electron tunnelling[14], non-contact friction [15] or atom rearrangements[16,17], even achieving atomic resolution[18]. In particular, the study of dissipation in *MFM* has been used to extract the *DC* susceptibility[19,20], distinguish between *Néel* and *Bloch* domain walls[6,21] , identify pinning sites[22] and obtain a three dimensional map of the sample stray field[23]. The energy-loss imaging is also a promising technique to characterize single magnetic nanoparticles[24,25]. In most of these cases, dissipation is associated to phenomena occurring in the sample although the loss of energy due to the reorientation of the tip magnetization can also be evaluated[23]. Nevertheless, the microscopic mechanisms behind the energy loss in minor hysteresis loops have been largely discussed in the literature[26] although they are still far from being fully understood [27].

In this work, we evaluate the energy losses occurring while measuring *MFM* in a CoNi multilayer film with strong perpendicular anisotropy. These effects are explained in terms of rotation of spins taking place at the apex of the *MFM* tip. Moreover the dissipated energy is analyzed as a function of the tip-sample distance –by using spectroscopic methods- for two different cases: attractive and repulsive interactions. Among the advantages of the spectroscopic method is the acquisition of several signals simultaneously without feedback influence [28]. An unexpected negative dissipation gradient is experimentally measured. Results obtained from micromagnetic simulations that show a good agreement with the experimental results are then introduced to support the explanation given.

Results and discussion

[a.] *Instituto de Ciencia de Materiales de Madrid-CSIC, 28049 Madrid (Spain)*
[b.] *Department of Physics, McGill University, Montreal, H3A 2T8 (Canada)*
[c.] *Departamento de Física de la Materia Condensada, Instituto Nicolás Cabrera and Condensed Matter Physics Center (IFIMAC), Universidad Autónoma de Madrid, 28049 Madrid, (Spain)*
[d.] *Donostia International Physics Center DIPC, Paseo Manuel de Lardizabal 4, 20018 Donostia-San Sebastián, (Spain)*
[e.] *IKERBASQUE, Basque Foundation for Science, 48013 Bilbao, Spain.*
† These authors contributed equally to this work
* email: aasenjo@icmm.csic.es; juanjo.saenz@dipc.org

Electronic Supplementary Information (ESI) available: [details of any supplementary information available should be included here]. See DOI: 10.1039/x0xx00000x

An MFM experiment is presented in Figure 1, in which the surface topography (Figure 1a) is mapped with the tip oscillating at constant amplitude (A_{osc}) at a tip-sample separation distance of few nm, where *van der Waals* forces are typically dominant. The topographic error signal and the shift in the oscillation frequency Δf (the latter accounting, to a first approximation, for the net force gradient sensed by the probe) are shown in Figures 1b and 1c, respectively. Upon tracking the topography, the tip-sample distance is increased by 30 nm so that magnetostatic interactions become dominant and the scan is then repeated (Figures 1e and 1f).

The average dissipated power during scanning probe experiments can be easily calculated[7] (see Supporting Information for more details), and the resulting dissipation maps for both the topographic and MFM scans are shown in Figures 1d and 1g, respectively. Dissipative processes occurring at low distances seem to be dominated by *van der Waals* interactions, as a strong correlation is observed between the dissipation map (Figure 1d) and the main feedback error (Figure 1b), although in the frequency shift image (Figure 1c) the magnetic domains mixed up with the topographic pattern. The operation mode close to the non-contact regime causes the tip to describe a trajectory along regions where different interactions are predominant and proves the strong magnetostatic interaction between tip and sample. During the *MFM* scan, the dissipation map reproduces the magnetic contrast (Figure 1e) to a very good extent, achieving a remarkable lateral resolution below 10 nm. Thus, energy dissipation at separations of tens of nm can be attributed to the magnetostatic coupling between both the tip and the multilayer.

Some interesting features can be observed in Figure 1e which have the same shape as the attractive domains (dark areas) but are slightly shifted from their positions to the bottom-right direction (a well-defined contour line around them can be observed). These features more easily recognized in Figure 1g might be caused by a sudden rotation of spins at the tip apex. The shape anisotropy of an *MFM* probe forces its spins to point along the tip axis, usually considered to be perpendicular to the sample surface (*Z* axis). During MFM experiments, a misalignment occurs between the sample stray field and the magnetization of the tip, so that for strong enough stray field, the magnetization can rotate away from its shaped induced position. This might eventually happen close to the central areas of the attractive domains where the magnetostatic coupling is higher (note that the scale bar in Figure 1f

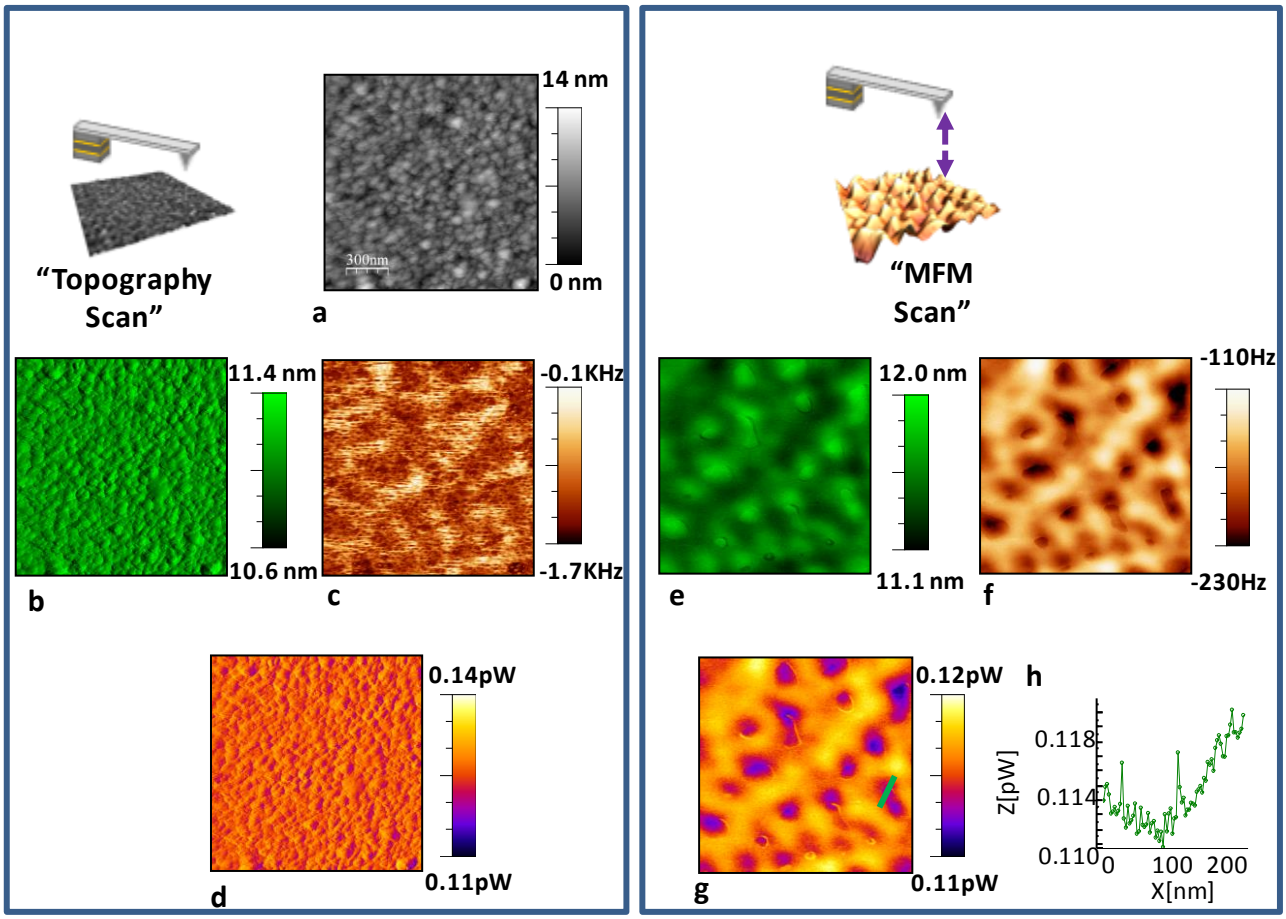

Fig. 1. (a) Topography and corresponding (b) & (e) oscillation amplitude, (c) & (f) frequency shift and (d) & (g) dissipation images of the CoNi multilayer. (a)-(d) were measured while tracking the topography and (e)-(g) correspond to the 30 nm lifted MFM scan. (h) Profile in the retrace dissipation image (g), showing a 5 fW peak.

corresponds to a force gradient of $5 \cdot 10^{-3}$ N/m), giving rise to an enhanced *MFM* contrast once the magnetic moments point parallel to the field. The highly dissipative contour lines indicate the transition regions where the effective magnetic stray field reaches the critical value[23], in such a way that the magnetization flips from the two configurations during one oscillation cycle in a hysteretic way.

According to the magnetic dissipation image shown in Figure 1g, attractive interactions yield less dissipative contrast. This can be explained thinking in terms of the system trying to reach a minimal *Zeeman* energy: the relatively small susceptibility of a sample that is close to its saturation state is expected to cause small power losses under the presence of an *AC* magnetic field (such as the one the *MFM* tip is subject to during an oscillation cycle), with minor loops that barely show hysteretic behaviour. On the contrary, larger susceptibilities are associated to the repulsive side of a hysteresis loop; thus, an *AC* field would induce a stronger damping in the cantilever oscillation while scanning over repulsive domains. *Grütter* and co-workers[8] realized the importance of the magnetization polarity with respect to the stray field direction and used it to explain dissipation maxima and minima in their results.

Keeping this idea in mind, we further studied the dependence of energy losses on distance by scanning the tip parallel to the sample surface (see Figure 2a) while gradually decreasing the separation distance *Z* down to contact [29]. Again, data on the oscillation amplitude and frequency shift were recorded (Figure 2b and 2c, respectively) and the dissipated power was calculated (Figure 2d). The evolution of all these parameters (A_{OSC}, Δf and ΔP) versus tip-sample distance can thus be analysed in detail. Note that no topographic feedback was enabled during the realization of this experiment so the tip starts tapping the surface for different *Z* values depending on the local roughness. In order to simplify the interpretation of *MFM* images, the horizontal axis on the profiles shown was renormalized so that zeros correspond to the distance at which the topography was recorded in Figure 1 [$A_{OSC}(z_{piezo}=0)$ = 11 nm].

First, we discuss the results for the case of repulsive interactions (black profiles in Figure 2b). The oscillation amplitude shows a light decrease by around 1 angstrom in the

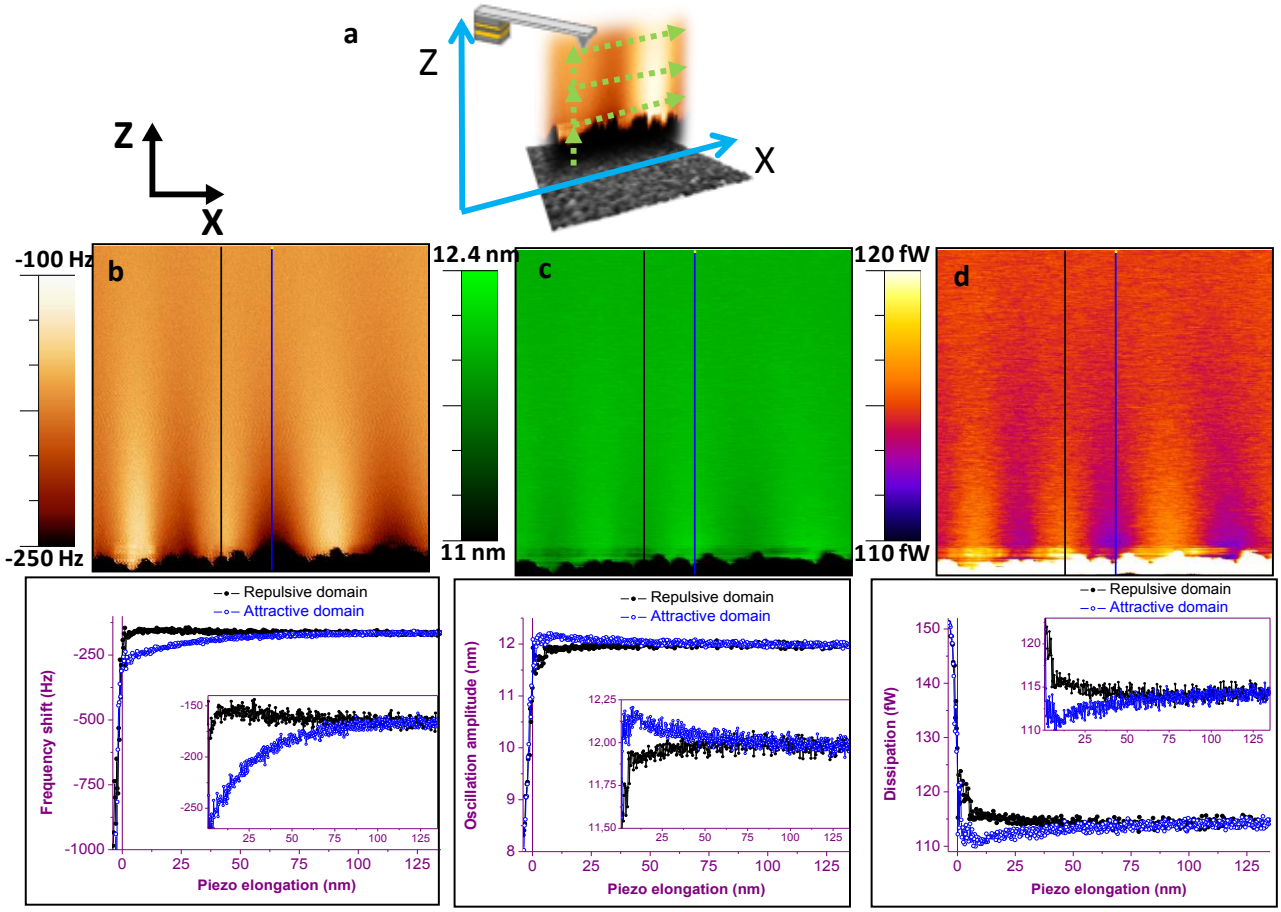

Fig. 2. (a) Scheme of the 3D mode measurement. The 3D modes measured scanning the tip 1.5 µm parallel to the sample (X) for a variable separation (Z) of 150 nm. (b) Frequency shift, (c) oscillation amplitude and (d) dissipated power images. Blue/black profiles give information on the dependence on distance over an attractive/repulsive domain. Insets show subtle trends on the curves. The horizontal axis were renormalized so that zero corresponds to the distance of the topographic feedback.

last 70 nm range displayed in the inset of Figure 2c, before the probe starts tapping on the surface. Similarly, the dissipation curve for repulsive interactions shows a slight increase of 1-2 fW as the tip approaches the surface (black profile in the inset of Figure 2d).

On the other hand, surprisingly in the case of attractive tip-sample interactions (blue profile in Figure 2b), an increase in A_{OSC} of up to 2 Å is recorded as the tip approaches the sample. This is a fingerprint of a negative dissipation gradient that is clearly observed when an attractive magnetostatic interaction is present (blue profiles in Figure 2d). This counterintuitive behaviour means that for a relatively large range of distances the closer the tip is to the sample, the less energy is needed to make it oscillate.

During one oscillation, the end of the tip is subject to minor cycles centred around a *DC* value in such a way that approaching the surface results in an enhanced *DC* biasing towards the saturation region of the loop. Under such circumstances, the area enclosed by the minor loop may decrease for lower tip-sample separations. However, a subtle consideration must be taken into account: even if the amplitude remained constant while approaching the surface, the field range that the probe is subject to would not. The stray field of the sample is not homogeneous but increases rapidly for low distances; therefore, the same amplitude becomes equivalent to larger field ranges. For the limit of very small oscillations and a dipolar sample, the field range applied during the minor hysteresis loop evolves as z^{-4}.

In order to get a theoretical estimation of the power dissipated by an *MFM* tip interacting with an out-of-plane (*OOP*) domain, micromagnetic simulations were performed using the finite difference *OOMMF* code (see Supporting Information). Two cases were considered, where the sample domain was oriented either parallel (↓↓) or anti-parallel (↓↑) to the magnetization in the tip and power losses of $P_{\downarrow\downarrow}$=1,2·10^{-3} fW and $P_{\downarrow\uparrow}$= 1,4·10^{-3} fW were obtained, respectively. As a consequence, larger power losses are predicted to take place when the sample domain points to the opposite direction, as was indeed observed experimentally. However, these calculated values differ by two orders of magnitude from the measured dissipation presented above. Since simulations are computing costly, only a limited number of spins flipping their orientation can be considered in them, thus underestimating the total losses occurring in the experiment. However, an experimental fingerprint of such a small group of spins are the dissipative contour lines mentioned before and observed in Figure 1g, where magnetic energy losses in the order of few fW were recorded (Figure 1h). This confirms the validity of the simulations in order to explain the energy dissipated by relatively small regions of the interacting tip. Furthermore, it supports our explanation for the observed negative dissipation gradients in hysteretic materials.

For this purpose, we last analyse in more detail the evolution of these dissipative contour lines versus tip-sample distance. Figure 3 presents again measured values of Δf (X,Z) and A_{OSC} (X,Z) and the calculated ones of ΔP(X,Z) in a region of the sample where several of those dissipative features were observed (note that in the results shown in Figure 2 they were not present due to the smaller interaction taking place, as demonstrated by the values of Δf). In this case, a lower A_{OSC} of

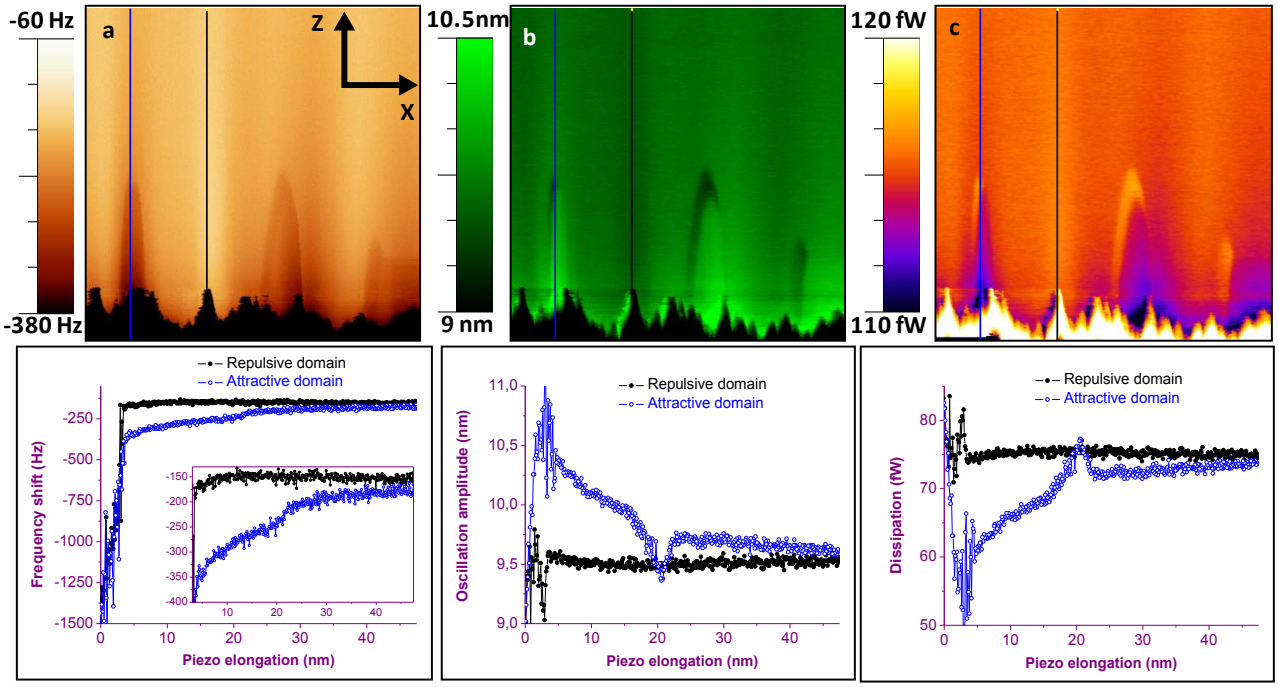

Fig. 3. 3D modes measured scanning 1.5 µm horizontally while sweeping the tip-sample distance by 60 nm. A bump and subsequent changes in the (a) frequency shift, (b) amplitude and (c) dissipation images (left column) and profiles in them (right column) are clearly visible.

9 nm was used. The parabolic cross sections of the regions subtended by these dissipative lines can be clearly distinguished. Data within this regions display stronger attraction, which becomes evident when comparing the blue profiles in Figures 3a and 2b. Furthermore, the amplitude grows by over 1 nm and power losses drop pronouncedly, after the probe has entered this region. The contour lines themselves appear as a bump in A_{OSC} and ΔP. This enhanced dissipation reflects the fact that the critical field condition – responsible of the spin switching at the tip apex – is fulfilled at some point during the oscillation cycle; this rotation of spins adds up some extra dissipation that, in the case of the results shown in Figure 3c, amounts to 7 fW, the same order of magnitude as the values given above. Leaving behind the transition and going well into the parabolic region gives rise to a considerably larger dissipation drop, as compared to the former situation described in Figure 2. This reflects a gradual reorientation of magnetic moments towards the sample stray field, instead of being sudden rotations. It is in this situation when the negative dissipation gradient becomes most evident, with a drop of around 30% while approaching the tip by 45 nm.

Although some dissipation is expected to take place at the sample, the most relevant contribution to dissipation is assumed to arise from the tip since its switching field was measured to be 4-5 times smaller than the sample one. This assumption is supported by the existence of those rings discussed above, as they yield constant dissipation contour lines that are most likely due to rotation of the same cluster of spins at the tip apex once a critical field is reached, rather than to groups of spins flipping in the magnetic sample[23].

Conclusions

In conclusion, the tiny amount of energy dissipated at the apex of an MFM tip under the influence of the sample stray field has been measured and its evolution with varying distance has been studied. As a main consequence, a counterintuitive behaviour of the dissipation versus the tip-sample distance was found for the case of domains with the magnetic moment parallel to the magnetization in the probe. Micromagnetic calculations yield a dissipation value in the order of few fW, which is in agreement with power losses caused by relatively small regions of spins flipping their magnetization. Large mutual influence reflects in much higher dissipations of the order of hundreds of fW. Comparable observations were obtained in a variety of samples with high stray field, by using different MFM probes and under different working conditions (see Figures 2-6 in Supplementary Information). Thus, in a broader perspective, it is possible to transfer this idea to analogous hysteretic tip-sample systems to gain information about the susceptibility or the energy product. In particular, a similar behaviour is expected for the case of ferroelectric materials with domains of opposite polarities, when using biased metallic probes, as long as the electrostatic mutual influence approaches the saturation regime of the hysteresis loops.

Experimental Section

The sample. The results shown in the manuscript correspond to a sample of CoNi/Pt multilayers with strong perpendicular anisotropy. The $Co_{50}Ni_{50}$ thin film 20nm thick was deposited by sputtering on a Si substrate with a Pt buffer layer of few nm. The macroscopic hysteresis loop measured by Vibrating Sample Magnetometry along the OOP direction yields a remanent magnetization of 87 % the saturation value, with a coercive field Hc=130kA/m. The average domain size imaged by MFM was about 150 nm in the demagnetized state.

MFM measurements. The same kind of commercial Nanosensors PPP-MFMR probe was used in all experiments shown in the letter although a variety of commercial and home-made probes have been used to explore the reproducibility of the effect. PPP-MFMR probes present an estimated spring constant k ≈ 1.6 N/m, a quality factor Q ≈ 150 and a natural resonance frequency f_0 ≈ 75 kHz. Its switching field was characterized by Variable Field Magnetic Force Microscopy and found to be about 29kA/m. The tip was placed in an effectively saturating magnetic field along its axial direction prior to the experiments shown.

The force gradient between tip and sample can be calculated as a function of the frequency shift (Δf), the resonance frequency and the spring constant by:

$$\left|{}^{\partial F}/_{\partial z}\right| = {}^{(\Delta f \cdot 2k)}/_{f_0} \quad (1)$$

A Cervantes system from Nanotec Electrónica was used, conveniently modified to apply OOP fields. The amplitude modulation mode was used, with the phase shift between the excitation and oscillation signals kept constant to 90^0 by means of a phase locked loop (PLL). Experiments shown here were carried out in ambient conditions and at room temperature; nevertheless, in order to reduce capillarity effects between the tip and the sample, a low humidity atmosphere (below 5%) was used. Moreover, in order to confirm the reproducibility of the effect another set of experiments have been performed in a different MFM system mounted on a high vacuum chamber. In this case, different control modes as Frequency Modulation or Drive Amplitude Modulation have been used. The values of the energy dissipated in all the experiments are similar.

It is worth pointing out that, in order to disregard eventual artefacts introduced by non-flat instrumental responses, the transfer function of the piezoacoustic excitation system was experimentally determined, as has been cautioned before [30,31], and no relevant contribution was found for the values shown above.

Acknowledgements

We gratefully thank funding from projects CSD2010-00024, MAT2013-48059 (MINECO). The authors want to thank E. Sahagún, M. Vázquez and J. Dancausa for successful discussion.

References

1 W.Wernsdorfer, E. B. Orozco, K. Hasselbach, A. Benoit, B. Barbara, N. Demoncy, A. Loiseau, H. Pascard, D. Mailly, *Phys. Rev. Lett., 1997*, **78** (9), 1791.

2 B. C. Stipe, H. J.Mamin, T. D. Stowe, T. W. Kenny, D. Rugar, *Phys. Rev. Lett., 2001*, **86**, 2874-2877.

3 D. Rugar, R. Budakian, H. Mamin, B. Chui, *Nature, 2004,* **430**, 329-332.

4 R. Wiesendanger, *Rev. Mod. Phys., 2009,* **81**, 1495.

5 Q. A.Pankhurst, J. Connolly, S. K. Jones, J. Dobson, *J. Phys. D: Appl. Phys., 2003*, **36**, R167-R181.

6 P. Grütter, Y. Liu, P. LeBlanc, U. Dürig, *Appl. Phys. Lett., 1997*, **71**, 279.

7 J. P.Cleveland, B. Anczykowski, A. E. Schmid, V. B. Elings, *Appl. Phys. Lett., 1998*, **72**, 2613.

8 R. García, R. Magerle, R Pérez, *Nature Materials, 2011*, **6**, 405-411.

9 J. J.Sáenz, N. García, P. Grütter, E. Meyer, H. Heinzelmann, R. Wiesendanger, L. Rosenthaler, H.R.Hidber, H.-J. Güntherodt, *J. Appl. Phys., 1987*, **62**, 4293.

10 Y.Martin, K. Wickramasinghe, *Appl. Phys. Lett., 1987*, **50**, 1455–1457.

11 R. García, N. F. Martínez, C. J. Gómez, A. García-Martín, *NanoScience and Technology*, Springer Berlin Heidelberg, 2007; pp361-371.

12 R. García, C.J. Gómez, N.F Martinez, S. Patil, C. Dietz, R. Magerle, *Phys. Rev. Lett., 2006*, **97**, 016103.

13 W. Denk, D. W. Pohl, *Appl. Phys. Lett., 1991*, **59**, 2171.

14 L. Cockins, Y. Miyahara, S.D. Bennett, A.A. Clerk, S. Studenikin, P. Poole, A. Sachrajda, P. Grutter, *Proc. Natl. Acad. Sci., 2010*, **107**, 9496-9501.

15 M. Kisiel, E. Gnecco, U. Gysin, L. Marot, S. Rast, E. Meyer,. *Nature Materials*, *2011*, **10**, 119-122.

16 N. Oyabu, P. Pou, Y. Sugimoto, P. Jelinek, M. Abe, S.Morita, R.Pérez, Ó. Custance, *Phys. Rev. Lett., 2006*, **96**, 106101.

17 H. J Hug, A. Baratoff, *Noncontact Atomic Force Microscopy. NanoScience and Technology*. Springer Berlin Heidelberg, 2002; pp 395-431.

18 R. Lüthi, E. Meyer, M. Bammerlin, A. Baratoff, L. Howald, Ch. Gerber, H.-J. Güntherodt, *Surf. Rev. Lett. 1997*, **4**, 1025.

19 E. Zueco, W. Rave, R. Schaefer, A. Hubert, L. Schultz, *J. Magn. Magn. Mater., 1998*, **190**, 42-47.

20 A. Thiaville, J. Miltat, J. M García, *Magnetic Microscopy of Nanostructures. NanoScience and Technology.* Springer Berlin Heidelberg, 2005; pp 225-251

21 Y. Liu, B. Ellman, P. Grütter, *Appl. Phys. Lett., 1997*, **71**, 1418-1420.

22 R. Proskch, K. Babcock, J. Cleveland, *Appl. Phys. Lett., 1999*, **74**, 419-421.

23 Ó. Iglesias-Freire, J. R. Bates, Y. Miyahara, A. Asenjo, P.H. Grütter, *Appl. Phys. Lett.*, *2013*, **102**, 022417.

24 B. Torre, G. Bertoni, D. Fragouli, A. Falqui, M. Salerno, A. Diaspro, R. Cingolani, A. Athanassiou, *Scientific Reports,* 2011, 1, 202.

25 C. Moya, O. Iglesias-Freire, N. Pérez, X. Batlle, A. Labarta, A. Asenjo, *Nanoscale,* 2015, 7, 8110-8114.

26 D.C. Jiles, Y. Melikhov, Modelling of Nonlinear Behaviour and Hysteresis in Magnetic Materials. *Handbook of Magnetism and Advanced Magnetic Materials,* Wiley Online Library, 2007.

27 A. Berger, S.Mangin, J. McCord, O. Hellwig, E. E. Fullerton, *Phys. Rev. B, 2010*, **82**, 104423.

28 E. Palacios-Lidon, C. Munuera, C.Ocal, J.Colchero, *Ultramicroscopy*, *2010*, **110**, 789–800,

29 C. Gómez-Navarro, A. Gil, M. Álvarez, P.J. De Pablo, F. Moreno-Herrero, I. Horcas, R. Fernández-Sánchez, J. Colchero, J. Gómez-Herrero, A.M. Baró, *Nanotechnology, 2002*, **13**, 314-317.

30 R. Proksch, S. V. Kalinin, *Nanotechnology 2010*, **21**, 455705.

31 A. Labuda, Y. Miyahara, L. Cockins, P. H. Grütter, *Phys. Rev. B, 2011*, **84**, 125433.